Calculating the energy spectrum and electronic structure of two holes in a pair of strained Ge/Si coupled quantum dots

A. I. Yakimov,* A. A. Bloshkin, and A. V. Dvurechenskii
Rzhanov Institute of Semiconductor Physics, Siberian Branch of the Russian Academy of Sciences, prospekt Lavrent'eva 13, 630090 Novosibirsk, Russia

(Received 21 December 2009; revised manuscript received 28 February 2010; published 19 March 2010)

We theoretically investigate the energy spectrum and electronic structure of two vertically stacked Ge/Si quantum dots loaded with a pair of interacting holes, and study the dependence of basic physical characteristics on dot size and interdot separation. In particular, we focus on the splitting of the lowest spin singlet and triplet states and spatial correlations between holes. Here the term "spin" is rather an index for two Kramers degenerate states. The two holes are treated by six-band $\mathbf{k}\cdot\mathbf{p}$ calculations combined with the configuration-interaction model taking into account the realistic situation when both Si matrix and Ge nanoclusters are inhomogeneously strained. It is shown that asymmetry of strain distribution and spin-orbit coupling of the valence band introduce characteristic features in both single- and many-particle hole states, which are not captured by the usual one-band heavy-hole approximation. We find a level anticrossing between the lowest singlet and triplet states with a zero anticrossing energy gap as a function of interdot spacing. It is demonstrated that the level anticrossing between many-particle states is accompanied by a level crossing between single-particle bonding and antibonding molecular orbitals. We argue that both phenomena of level crossing and anticrossing originate from the asymmetry-induced localization of single-particle hole wave functions on different dots. Above a certain dot separation, the Mott-type delocalized-to-localized transition for the many-particle hole states is observed. We show that the transition is caused by the combined action of correlations and strain asymmetry.

DOI: 10.1103/PhysRevB.81.115434 PACS number(s): 73.21.La, 73.20.At, 71.55.Cn, 81.07.Ta

I. INTRODUCTION

The three-dimensional quantum confinement of conduction electrons or valence holes in quantum dots (QDs) leads to the formation of a discrete carrier energy spectrum, resembling that of an atom. Coupled quantum dots represent another example of a zero-dimensional system in which the interdot coupling extends the analogy between QDs and natural atoms to artificial and natural molecules. Recently considerable interest has been devoted to double QDs occupied by two electronic spins. Quantum computation requires coherent coupling between the dots and the coherence to be preserved on sufficiently long-time scales. The spin degrees of freedom (rather than charge) are of special interest for information processing since they can take advantage of the comparatively long spin-coherence time and, hence, can serve as the quantum bits (qubits).[1–4] It has been established that a set of gates that consists of all one-bit gates and two-bit XOR gate is universal, and all unitary operations can be expressed as compositions of these gates.[5] The two-dot systems provide the necessary two-qubit entanglement required for the basic gate manipulation. Loss and DiVincenzo[1] suggested a scheme in which the two-qubit operations are performed on the physical qubits (individual spins) by controlling the Heisenberg exchange interaction in a double QD, which is characterized by the singlet-triplet energy splitting J_{ST}.[1] Some important aspects of singlet-triplet splitting, correlations, and entanglement of two electrons in quantum-dot molecules have been discussed in Refs. 6–11.

The key requirement is that the lifetime of the spin is long compared with the time required for the operation of logic gates. Until now electron-spin dynamics have attracted by far the most attention since theoretical approaches to the two-electron problem is more mature.[12–15] However, it has become clear that spatially inhomogeneous coupling of nuclei via the hyperfine interaction to the electron spin results in rapid spin dephasing (see, Ref. 16, and references therein). Because the valence band couples more weakly to the nuclear spins, hole spin dynamics can be extremely slow[17] demonstrating features that are quite different from the electron-spin relaxation.[18] Moreover, as shown recently,[19] the problem of coherent manipulation of hole spin can be circumvented by making use of electric dipole spin-resonance technique instead of standard electron-spin resonance for electrons. Therefore, the case of two holes confined in a pair of coupled QDs deserves special attention. The two-hole problem is more complicated that for electrons. Unlike conduction band, valence states in typical semiconductors are derived from p-type atomic orbitals of the semiconductor lattice and, hence, the holes experience a strong spin-orbit interaction. The spin-orbit interaction couples the hole orbital angular momentum $\mathbf{L}$ and its spin $\mathbf{S}$ so the hole states cannot be classified by their spin but rather a total angular momentum $\mathbf{J}=\mathbf{L}+\mathbf{S}$. The p-like valence states have $L=1$, giving $J=\frac{3}{2}$ or $J=\frac{1}{2}$. The states $|\frac{3}{2},\pm\frac{3}{2}\rangle$ and $|\frac{3}{2},\pm\frac{1}{2}\rangle$ correspond to the heavy-hole (HH) and the light-hole (LH) bands, respectively. The states $|\frac{1}{2},\pm\frac{1}{2}\rangle$ correspond to the split-off (SO) band. Here $|J,J_z\rangle$ are the eigenstates of the total angular momentum J and its z projection J_z. Recently the procedure of wave-function expansion in the basis $|J,J_z\rangle$ has been performed both for single[20] and double[21,22] Ge/Si QDs whose size is about 10 nm. The contribution of the states with $J_z=\pm\frac{3}{2}$ turns out to be predominant and amounts to 85–90 % for the ground and first excited state while the rest part be-

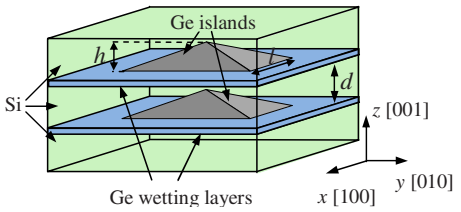

FIG. 1. (Color online) Schematic picture of a Ge/Si double QD used for simulation of hole states.

longs to the $\pm\frac{1}{2}$ states (the light and split-off states). Although the admixture of minor components does not exceeds 15%, it can be sufficient to substantially alter the symmetry of hole states in coupled QDs.[21–25]

In the two-particle electron problem, where spin-orbit interaction is negligible, the two-electron wave functions can be systematized as either spin singlet or triplet since the spatial and spin part separate. In the case of two holes, however, such a separation is, in general, no longer possible. Nevertheless one can consider the projection of the angular momentum J_z as an analog of electron spin for hole states (i.e., the effective spin[20,26] or pseudospin[27,28]) and classify the two-hole states as the effective spin singlet or triplet. Since the pseudospins of holes interact exactly the same way as spins of electrons[29] all the quantum gates proposed to be implemented with electrons can be done with holes. In this paper, we calculate the exchange coupling as the energy difference between the ground and first excited many-body states in double Ge/Si QDs: $J_{ST}=E_{\text{singlet}}-E_{\text{triplet}}$, where "singlet" and "triplet" refer to the effective spin symmetry of the two-hole wave function. We employ the configuration-interaction method to describe two-hole states and are interesting in the evolution of J_{ST} and other basic physical characteristics as the interdot distance and dot size are varied.

II. MODEL

A. Double-dot geometry

We consider two *identical* vertically aligned pyramidal Ge nanoclusters with four {105}-oriented facets and a (001) base embedded into the Si matrix as shown in Fig. 1. Each pyramid lies on a 4 ML Ge wetting layer. The nanoclusters are separated by a Si barrier of thickness d measured from wetting layer to wetting layer. The pyramid base length l is varied from 10 to 20 nm in different calculations; the pyramid aspect ratio h/l is fixed and equal to 0.1. The shape and size for our dot molecules are inspired from the experimental studies of self-assembled Ge/Si QDs.[30] Epitaxial self-assembled QDs are commonly obtained by the Stranski-Krastanov growth mode.[31] The typical size of computational cell (Ge wetting layers plus Ge islands plus Si environment) is 17.5 nm × 17.5 nm × 62.5 nm along x, y, and z axes, respectively. In order to check whether the calculation volume is large enough to give the proper (size-independent) result, we performed numerical analysis also for different vertical sizes of computational domains ranging from 37.5 to 73 nm and found that the hole binding energy does not depends on the size of supercell to within <1 meV of accuracy.

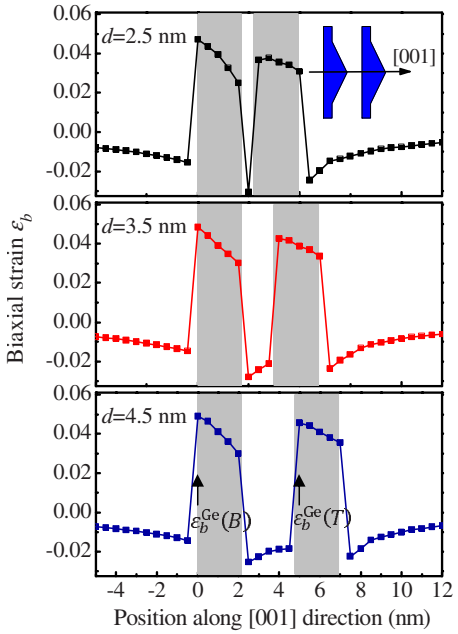

FIG. 2. (Color online) Biaxial component of the strain tensor for three selected interdot distances d as a function of the position along the [001] direction (given in the inset of the top panel). The origin of the horizontal coordinates corresponds to the lower boundary of the lowest Ge wetting layer. The shaded regions correspond to Ge pyramids and wetting layers. The dot base length l is 20 nm.

B. Strain calculation

We study a realistic situation when both Si matrix and Ge nanoclusters are inhomogeneously strained due to the ~4% lattice mismatch between Si and Ge. The finite-element calculations of three-dimensional spatial distribution of strain components $\varepsilon_{\alpha\beta}$ are performed using the package COMSOL MULTIPHYSICS with the approach described in Ref. 32. The strain-tensor elements are subsequently used as input to a strain-dependent Hamiltonian.

From our calculations we observe that the biaxial component of strain $\varepsilon_b=\varepsilon_{zz}-0.5(\varepsilon_{xx}+\varepsilon_{yy})$ is positive in the Ge wetting layer and QDs and negative in the Si layer separating the dots (Fig. 2). The hydrostatic strain $\varepsilon_h=\varepsilon_{xx}+\varepsilon_{yy}+\varepsilon_{zz}$ (not shown here) resides entirely inside the dots and is approximately the same for the double-dot structures and the single dot.[21,33] In Fig. 3(a), we plot the biaxial deformation in the Ge top and bottom dots at the positions indicated by arrows in Fig. 2. Unlike the hydrostatic component, the biaxial strain inside QDs is decreased when the two dots are brought closely together. Furthermore, ε_b is different on both geometrically identical dots due to the lack of inversion symmetry with respect to the medium plane between the dots (the top-bottom symmetry), ε_b in the bottom dot is larger than in the top dot. The strain asymmetry $\Delta\varepsilon_b=\varepsilon_b^{\text{Ge}}(B)-\varepsilon_b^{\text{Ge}}(T)$ is found to be enhanced as the dot size is increased and falls down with d as the dots do no longer feel each other though the superimposed strain fields [Fig. 3(b)]. The asymmetry parameter $\Delta\varepsilon_b$ can be fitted as $\Delta\varepsilon_b=\Delta\varepsilon_b(0)\exp(-d/d_\varepsilon)$ with $\Delta\varepsilon_b(0)=0.037\pm0.002$, 0.035 ± 0.002, and 0.034 ± 0.05, $d_\varepsilon=1.92\pm0.03$ nm, 1.49 ± 0.03 nm, and 1.16 ± 0.08 nm for

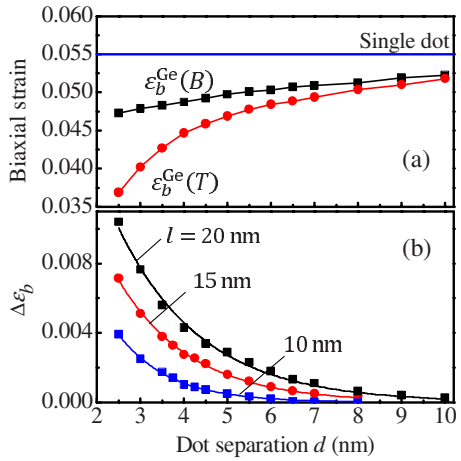

FIG. 3. (Color online) (a) Biaxial component of the strain tensor at the positions indicated by arrows in Fig. 2 as a function of dot spacing for $l=20$ nm. $\varepsilon_b^{Ge}(B)$ and $\varepsilon_b^{Ge}(T)$ are the maximum strain in Ge bottom and top dots, respectively. As reference, ε_b for the single-dot system is also shown by the horizontal line. (b) The difference between the strain on bottom and top dots, $\Delta\varepsilon_b=\varepsilon_b^{Ge}(B)-\varepsilon_b^{Ge}(T)$, as a function of d and l. The solid lines in (b) are fits to the data with the exponential functions $\Delta\varepsilon_b=\Delta\varepsilon_b(0)\exp(-d/d_\varepsilon)$ (see the text).

$l=20$ nm, 15 nm, and 10 nm, respectively. Note that the characteristic decay length d_ε is on the order of the vertical stress source dimension h, where $h=l/10$ is the dot height.

C. Single-particle states

Strained Ge/Si(001) layers represent heterostructures of the second type in which charge carriers of different signs are separated by the heterointerface; holes are localized in Ge nanoclusters and electrons are in the delocalized states of the conduction band of Si. The initial ingredients of our calculations are the single-particle energies and wave functions. So we start with determination of single-hole states. The single-particle hole energy levels and wave functions are obtained using a six-band $\mathbf{k}\cdot\mathbf{p}$ approximation, based on the method of Bir and Pikus,[34] which includes spin-orbit and strain effects. The coupling between the conduction and the valence bands is very small ($\sim$0.5%),[20] and it is not considered here. As opposed to Refs. 25 and 35, we include the SO band in our model because the effective mass of the split-off states in Ge is comparable with that of LHs. In addition, in small quantum dots, the spin-orbit splitting of the valence bands can be comparable to the quantization energy of holes and therefore cannot be neglected. The resulting hole eigenstates are six-component spinors with an admixture of two HH states, two LH and two SO states. The single-particle $\mathbf{k}\cdot\mathbf{p}$ Hamiltonian consists of four components,

$$H = H_{vv} + H_{so} + H_{strain} + \Delta E_v, \tag{1}$$

where H_{vv} contains terms which depend on wave vector $\mathbf{k}$, H_{so} describes spin-orbit interaction, H_{strain} is the strain-dependent contribution, and ΔE_v accounts for the average valence-band offset at the Ge/Si heterojunction. The detailed form of the Hamiltonian terms was given in Ref. 22.

In what follows we restrict ourselves to the two lowest hole states, σ_g and σ_u, made of symmetric and antisymmetric combination of the s-like single-dot orbitals. As mentioned before, there is no inversion center in the double quantum dots under consideration. So the hole eigenstates have not symmetric or antisymmetric parity in the full sense. Nevertheless we will follow the usual practice calling the σ_g and σ_u molecular orbitals by bonding (almost symmetric) and antibonding (almost antisymmetric) states,[7,8,23,36–38] correspondingly, although these names are not really justified.

D. Many-particle states

Based on single-particle orbitals obtained above, a configuration-interaction (CI) calculation can then be built. The CI method includes the effects of direct Coulomb interaction among charge carriers, exchange, and correlation due to interconfiguration coupling. As compared to single-configuration (SC) approaches such as Hartree-Fock[39,40] and local spin density,[41,42] the CI treatment will lead to a more faithful and accurate description of the actual two-particle wave functions in the double-dot system.[3,6–8] The many-body Hamiltonian can be written as

$$H = \sum_{i\sigma} E_i \psi_{i\sigma}^\dagger \psi_{i\sigma} + \frac{1}{2}\sum_{ijkl}\sum_{\sigma,\sigma'} \Gamma_{kl}^{ij} \psi_{i\sigma}^\dagger \psi_{j\sigma'}^\dagger \psi_{k\sigma'} \psi_{l\sigma}, \tag{2}$$

where E_i and ψ_i are the single-particle hole energy levels and corresponding molecular orbitals, respectively, σ and σ' are the indices of effective spin,

$$\Gamma_{kl}^{ij} = \int\int d\mathbf{r}_1 d\mathbf{r}_2 \frac{\psi_i^*(\mathbf{r}_1)\psi_j^*(\mathbf{r}_2)\psi_k(\mathbf{r}_2)\psi_l(\mathbf{r}_1)}{\epsilon(\mathbf{r}_1,\mathbf{r}_2)|\mathbf{r}_1-\mathbf{r}_2|}. \tag{3}$$

$\epsilon(\mathbf{r}_1,\mathbf{r}_2)$ is the position-dependent dielectric function. Here $V_{ij}=\Gamma_{ji}^{ij}$ and $K_{ij}=\Gamma_{ij}^{ij}$ represent diagonal Coulomb and exchange integrals, respectively, while the remaining terms are scattering terms. To solve the many-body problem we use the reduced CI treatment with σ_g and σ_u single-particle orbitals and ignoring π states built from the p-like single-dot wave functions. This approach has been shown to be reliable to calculate the lowest two-particle electronic states in coupled QDs.[8] The configuration-interaction approach consists of directly diagonalizing the Hamiltonian represented on a basis of Slater determinants. The many-body wave functions Ψ are written as linear combination of these determinants. For reduced CI problem, the Slater determinants are $|\sigma_g^\uparrow\sigma_u^\uparrow\rangle$, $|\sigma_g^\downarrow\sigma_u^\downarrow\rangle$, $|\sigma_g^\uparrow\sigma_u^\downarrow\rangle$, $|\sigma_g^\downarrow\sigma_u^\uparrow\rangle$, $|\sigma_g^\uparrow\sigma_g^\downarrow\rangle$, and $|\sigma_u^\uparrow\sigma_u^\downarrow\rangle$, where $|\sigma_i^{\uparrow(\downarrow)}\sigma_j^{\uparrow(\downarrow)}\rangle$ are the products of single-particle molecular orbitals $|i^{\uparrow(\downarrow)}\rangle$ and $|j^{\uparrow(\downarrow)}\rangle$, $i,j=g$ or u; g and u specify the symmetry under inversion with respect to the center of the molecule. The eigenfunctions σ_g and σ_u are a mixture of six components: spin-up and spin-down heavy-hole, light-hole, and split-off states. We use $\uparrow$ and $\downarrow$ to denote the orientations of the hole effective spin and assign an eigenstate $|\uparrow\rangle$ to be spin up if the spin-up components are larger than the spin-down ones. In this basis set, Eq. (2) transforms to the following form:[8]

$$H = \begin{pmatrix} E_g + E_u + V_{gu} - K_{gu} & 0 & 0 & 0 & 0 & 0 \\ 0 & E_g + E_u + V_{gu} - K_{gu} & 0 & 0 & 0 & 0 \\ 0 & 0 & E_g + E_u + V_{gu} & -K_{gu} & -\Gamma_{gg}^{gu} & -\Gamma_{uu}^{gu} \\ 0 & 0 & -K_{gu} & E_g + E_u + V_{gu} & \Gamma_{gg}^{gu} & \Gamma_{uu}^{gu} \\ 0 & 0 & -\Gamma_{gu}^{gg} & \Gamma_{gu}^{gg} & 2E_g + V_{gg} & \Gamma_{uu}^{gg} \\ 0 & 0 & -\Gamma_{gu}^{uu} & \Gamma_{gu}^{uu} & \Gamma_{gg}^{uu} & 2E_u + V_{uu} \end{pmatrix}. \quad (4)$$

In our work, we will use the conventional molecular notation of two-particle states: ${}^1\Sigma_g^{(a)}$ labels the ground-state singlet, ${}^1\Sigma_u$ and ${}^1\Sigma_g^{(b)}$ are excited singlet states, and ${}^3\Sigma_u$ corresponds to the lowest triplet state.

III. RESULTS AND DISCUSSION

A. Single-band approximation

In order to demonstrate that mixing of valence subbands is a key phenomena responsible for the characteristic behavior of two holes on double QDs, we first make single-band calculation with including the heavy-hole states only. As in Refs. 26 and 27, in this case it is convenient to identify $J_z = +\frac{3}{2}$ with the $\tilde{s}_z = +\frac{1}{2}$ pseudospin-up state and $J_z = -\frac{3}{2}$ with $\tilde{s}_z = -\frac{1}{2}$ pseudospin-down state. Since this approach ignores spin-orbit coupling, the single-band results are expected to be similar to those obtained in double QDs for electrons.[6–8] The data for QDs with the lateral dot size $l = 10$ nm are presented in Fig. 4.

The localization of single-hole states is illustrated in Fig. 4(a) where we plot the probabilities to find the hole occupying bonding or antibonding states inside the bottom or the top dot volume Ω_η, $p_{\eta,i} = \int_{\Omega_\eta} d^3r |\psi_i|^2$. Here η denotes the bottom ($\eta = B$) or the top ($\eta = T$) dot, $\psi_i = \sigma_g$ or σ_u. The data are obtained by numerical integration of hole wave functions over each dot. All probabilities are comparable (~40%) for all interdot distances, suggesting a covalentlike molecular states extended quasiequally in both dots. The bonding (antibonding) states are slightly more localized on the bottom (top) dot. As discussed in Refs. 7 and 33, the weak asymmetry appearing in Fig. 4(a) is caused by the asymmetry of strain-field distribution in the double-dot system (Figs. 2 and 3).

Some important diagonal matrix elements are shown in Fig. 4(b). Here V_{gg} denotes the direct Coulomb interaction between two holes occupying the bonding state, V_{gu} and K_{gu} describe the direct and exchange Coulomb interactions between one hole in the bonding and another in the antibonding states, respectively. Since V_{gg} and V_{uu} are identical, we plot only V_{gg}. When d increases, a general decrease in V_{gg} and V_{gu} and increase in K_{gu} is expected,[6,8] and this trend can be seen in Fig. 4(b).

We find that the ground two-hole state is the singlet ${}^1\Sigma_g^{(a)}$, followed by the threefold-degenerated triplet states ${}^3\Sigma_u$ and the next singlets ${}^1\Sigma_u$ and ${}^1\Sigma_g^{(b)}$. In Fig. 4(c), we decompose the ground two-hole state into the leading configurations. At small dot separation, both holes occupy bonding state and the dominant configuration is $|\sigma_g^\uparrow \sigma_g^\downarrow\rangle$. With increasing d, the bonding σ_g and antibonding σ_u orbitals tend to be degener-

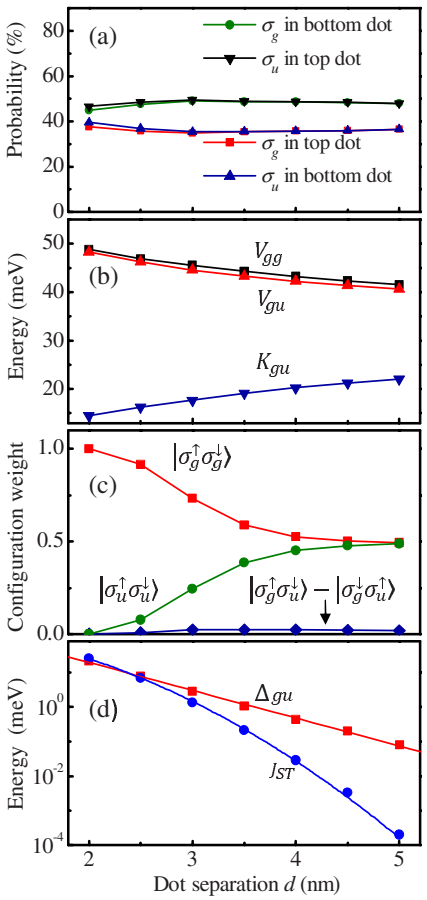

FIG. 4. (Color online) (a) The probability of finding the hole inside the bottom or the top dots in bonding (σ_g) and antibonding (σ_u) states. Note the total probability for each state $p_B + p_T$ is not equal to 100% because a part of the hole states reside in the Si barrier. (b) Diagonal Coulomb (V_{gg}, V_{gu}) and exchange (K_{gu}) integrals obtained with Eq. (3). (c) The weights of prototypical configurations for the two-hole ground state ${}^1\Sigma_g^{(a)}$. (d) The bonding-antibonding splitting $\Delta_{gu} = E(\sigma_g) - E(\sigma_u)$ and singlet-triplet splitting $J_{ST} = E({}^3\Sigma_u) - E({}^1\Sigma_g^{(a)})$ (symbols). The solid lines in panel (d) are fits to the data with $\Delta_{gu} = 1.03 \exp(-d/0.51)$ eV and $J_{ST} = 0.22 \exp[-(d/1.34)^2]$ eV. The results shown were obtained using a single-band approximation (no band mixing) applied to double Ge/Si QDs with the lateral size $l = 10$ nm.

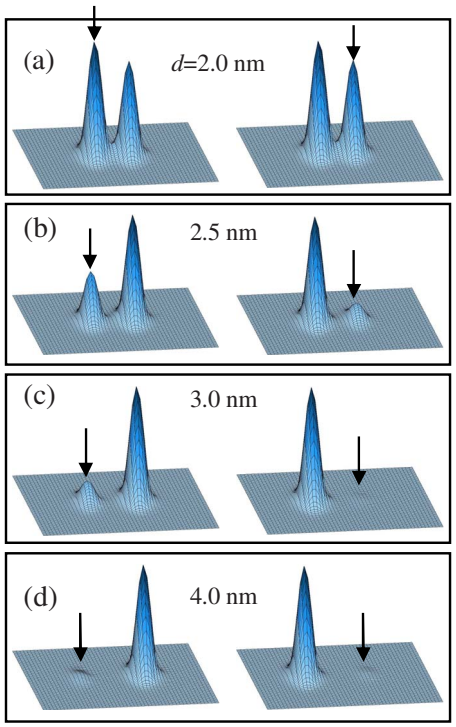

FIG. 5. (Color online) Spatial distributions of the pair-correlation functions in the (yz) plane calculated from single-band model for the ground-state singlet ${}^1\Sigma_g^{(a)}$ at (a) $d=2.0$ nm, (b) $d=2.5$ nm, (c) $d=3.0$ nm, and (d) $d=4.0$ nm. On the left-hand side, the first hole is fixed at the maximum of the charge density of the bottom dot while on the right-hand side, the first hole is fixed at the maximum of the charge density of the top dot, as indicated by the arrows.

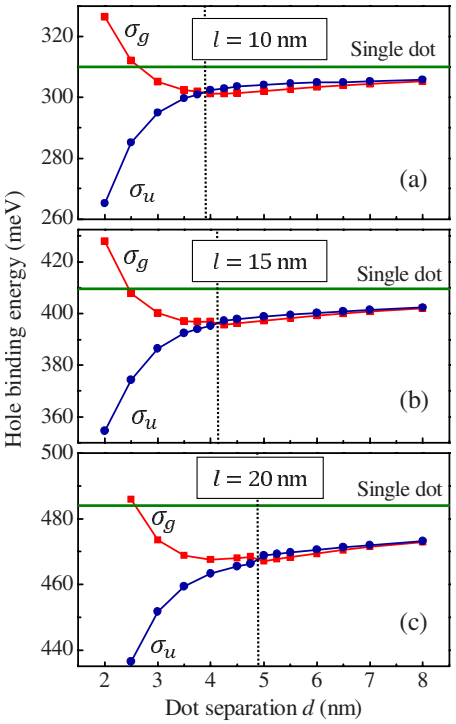

FIG. 6. (Color online) Evolution of hole binding energy in bonding and antibonding states as a function of the distance between QDs, calculated for (a) $l=10$ nm, (b) $l=15$ nm, and (c) $l=20$ nm with a 6×6 $\mathbf{k}\cdot\mathbf{p}$ model. As reference, the hole ground-state energy of the isolated single dot is also shown by the horizontal lines. All energies are counted with respect to the valence-band edge in bulk Si. The vertical dot lines are used to indicate the distance d_c at which the ground-state symmetry changes.

ate, and the ${}^1\Sigma_g^{(a)}$ state becomes a mixture of $|\sigma_g^\uparrow\sigma_g^\downarrow\rangle$ and $|\sigma_u^\uparrow\sigma_u^\downarrow\rangle$ determinants with a small contribution of the $|\sigma_g^\uparrow\sigma_u^\downarrow\rangle - |\sigma_g^\downarrow\sigma_u^\uparrow\rangle$ configuration.

Figure 4(d) shows the bonding-antibonding splitting $\Delta_{gu}=E(\sigma_g)-E(\sigma_u)$ between the single-particle molecular orbitals as well as the splitting between the ground-state singlet and triplet $J_{ST}=E({}^3\Sigma_u)-E({}^1\Sigma_g^{(a)})$. The energy gap Δ_{gu} is positive implying that the bonding orbital remains the molecular ground state at any d. Both Δ_{gu} and J_{ST} decay approximately exponentially as interdot separation increases and as the probability of the tunneling through the potential barrier goes to zero. The bonding-antibonding splitting can be fitted as $\Delta_{gu}=1.03\exp(-d/0.51)$ eV while the exchange energy varies as $J_{ST}=0.22\exp[-(d/1.34)^2]$ eV [solid lines in Fig. 4(d)], as expected for electrons from a simple analytical Heitler-London model.[2]

To examine the spatial symmetry of many-particle states $\Psi(\mathbf{r}_1,\mathbf{r}_2)$, we analyze in addition to the energy spectrum also the pair-correlation functions. The pair-correlation function is defined as $\rho(\mathbf{r}_0,\mathbf{r})=|\Psi(\mathbf{r}_0,\mathbf{r})|^2$ and shows how the position of one particle fixed at $\mathbf{r}_0$ affects the spatial distribution of the other particle. The data for the ground-state singlet ${}^1\Sigma_g^{(a)}$ are plotted in Fig. 5. At small dot spacing, the lowest singlet state clearly exhibits no spatial correlations among the two holes: the loading of one hole on one dot does not change the probability of finding the other one in any of the dots. In this case, the two holes are delocalized into both dots, thereby lowering their single-particle energy at the expense of Coulomb repulsion between holes. However, with increasing dot separation, the Mott-type delocalized-to-localized transition is observed: the two particles tend to occupy the opposite QDs, showing correlation-induced localization. In contrast, for the ${}^3\Sigma_u$ triplet state (not shown here), the two holes are localized on different dots at all interdot distances.

Summarizing results of this section we may conclude that the single-band treatment of two correlated holes reproduces well the basic physical regularities of two-electron systems.[6–8]

B. Multiband calculations

Now we take into consideration that the hole spin is really a spinor orientation,[23,24] although it is dominated by the $\frac{3}{2}$ heavy-hole contribution to the spinor. When the band mixing is included into the problem we obtain a behavior quite different from that depicted in Fig. 4.

In Fig. 6, we show the energies of σ_g and σ_u states calculated for QDs of different sizes l using a six-band $\mathbf{k}\cdot\mathbf{p}$ model. The most interesting property of this spectrum is that the change in dot separation d causes crossing between the energy levels corresponding to bonding and antibonding orbitals. As a result, at $d>d_c=(3.8-4.8)$ nm the antibonding

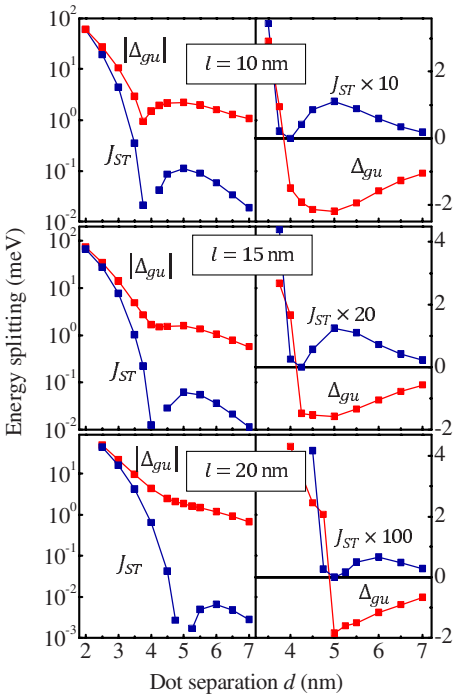

FIG. 7. (Color online) The energy gap between bonding and antibonding states $\Delta_{gu}=E(\sigma_g)-E(\sigma_u)$ and singlet-triplet splitting $J_{ST}=E(^3\Sigma_u)-E(^1\Sigma_g^{(a)})$ plotted in semilogarithmic scale (left-hand side) and in linear scale (right-hand side) as a function of dot separation d and dot base length l. Note that in the left panels, the absolute value of Δ_{gu} is displayed. The dips show the single-particle crossing and many-particle anticrossing points.

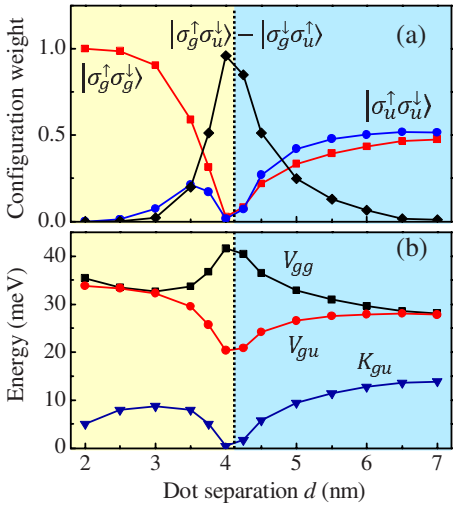

FIG. 8. (Color online) (a) The weights of prototypical configurations for the two-hole ground state $^1\Sigma_g^{(a)}$. (b) Diagonal Coulomb (V_{gg}, V_{gu}) and exchange (K_{gu}) integrals obtained with Eq. (3). V_{uu} is identical to V_{gg} and therefore is not plotted. The vertical dot lines indicate the distance d_c at which the orbital character of single-particle ground state switches from bonding to antibonding. The data are calculated using a six-band approximation applied to double Ge/Si QDs with $l=15$ nm.

molecular ground state appears and Δ_{gu} becomes negative (Fig. 7). Several explanations for the bonding-antibonding ground-state transition have been proposed.[21–24,36,37] Climente *et al.*,[23,24] considering the valence-band holes as 4 $\times$4 Luttinger spinors, ascribed this effect to the spin-orbit interaction of holes. Bester and Zunger[36] and Jaskólski *et al.*,[37] based on atomistic calculations, suggested that the negative value of Δ_{gu} originates from the *p*-type atomic orbitals responsible for the hole tunneling between the dots. We demonstrated that the reordering of bonding and antibonding states with increasing interdot distance is caused by the interplay of elastic strain effects and subband mixing.[21,22] The antibonding molecular ground state has been recently observed experimentally in two vertically stacked InAs/GaAs QDs using magnetophotoluminescence spectroscopy.[24]

In Fig. 7, we show the calculated values of bonding-antibonding and singlet-triplet splittings for double QDs of different size l. At large d, parameters Δ_{gu} and J_{ST} demonstrate quite different behavior. The singlet-triplet splitting is strongly reduced as the dot size increases while the bonding-antibonding splitting remains approximately the same. The exchange energy is determined by both the Coulomb interaction and the tunneling of holes between the dots. Since the effective potential barrier for holes is higher for larger dots due to the deepening of hole levels (Fig. 6), the quantum-mechanical coupling and hence J_{ST} eventually decreases with increasing l. On the contrary, in the weak-coupling region Δ_{gu} originates rather from asymmetry of strain distribution in the bottom and top dots than from tunneling coupling (see further discussion and Ref. 21) and therefore is less sensitive to l. The picture differs from that described above for small dot separation d. The result of bonding-antibonding and singlet-triplet splitting includes two competing effects. On one hand, large dot height h reduces the effective distance between the two dots and hence enlarges the coupling between them. (Note that interdot distance d is measured from wetting layer to wetting layer.) On the other hand, the hole energy levels are deeper in large dots, leading to a higher tunneling barrier, thus decreasing coupling. A weak dependence of both Δ_{gu} and J_{ST} on l (or on h) at $d \sim h$ is a consequence of this competition

Several remarkable features of two-hole states are revealed around the critical dot separation d_c at which the single-particle ground-state symmetry switches from bonding to antibonding. This behavior can be considered as *anomalous* as it cannot be inferred from single-band approximation and is not observed for two-electron states. The data are shown in Fig. 7 for $l=10$, 15, and 20 nm, and in Figs. 8 and 9 for $l=15$ nm. Results for $l=10$ nm and $l=20$ nm are quite similar. We find that (i) in the vicinity of d_c, the singlet-triplet splitting drops rapidly to zero and then restores again (Fig. 7). This suggests the possibility of turning off the exchange interaction. The coincidence of the points of single-particle level crossing and many-body level anticrossing allows us to suppose that these phenomena are of the same origin.

(ii) Except the region of $d \sim d_c$,[43] the ground state is the singlet $^1\Sigma_g^{(a)}$ followed by the threefold-degenerated triplet $^3\Sigma_u$. However, the character of the $^1\Sigma_g^{(a)}$ state is very different at different dot separation [Fig. 8(a)]. At small d, the wave-function analysis reveals a dominant contribution from

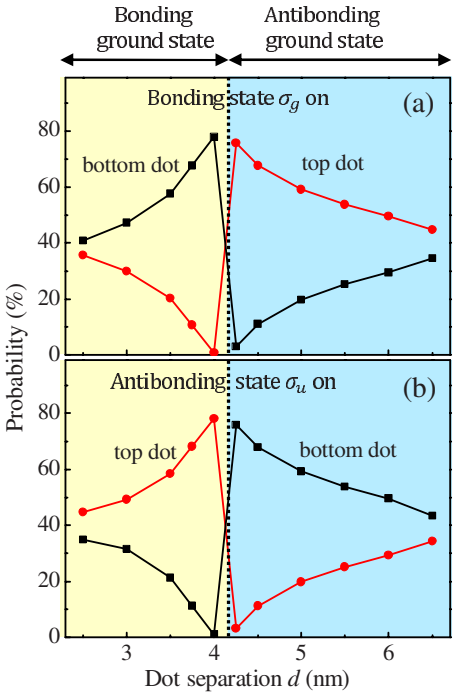

FIG. 9. (Color online) The probability of finding a hole inside the bottom or the top dots in (a) bonding and (b) antibonding states for double Ge/Si QDs with $l=15$ nm. Different background colors signify the regions of different single-particle ground-state symmetry.

the product of two delocalized molecular orbitals $|\sigma_g^{\uparrow}\sigma_g^{\downarrow}\rangle$. At large d, where the antibonding orbital is the ground single-particle state, the ${}^1\Sigma_g^{(a)}$ singlet becomes a mixture of $|\sigma_g^{\uparrow}\sigma_g^{\downarrow}\rangle$ and $|\sigma_u^{\uparrow}\sigma_u^{\downarrow}\rangle$ configurations with dominating $|\sigma_u^{\uparrow}\sigma_u^{\downarrow}\rangle$ determinant. At the critical point, contributions of both $|\sigma_g^{\uparrow}\sigma_g^{\downarrow}\rangle$ and $|\sigma_u^{\uparrow}\sigma_u^{\downarrow}\rangle$ disappear and the ${}^1\Sigma_g^{(a)}$ state turns out to be the pure $|\sigma_g^{\uparrow}\sigma_u^{\downarrow}\rangle - |\sigma_g^{\downarrow}\sigma_u^{\uparrow}\rangle$ state.

(iii) The self-Coulomb energies of the σ_g and σ_u orbitals (V_{gg} and V_{uu}) enhance around d_c while the Coulomb and exchange energies between σ_g and σ_u orbitals (V_{gu} and K_{gu}) are minimum at the anticrossing point [Fig. 8(b)]. The exchange integral K_{gu} is reduced even down to zero.

To interpret suppression of singlet-triplet splitting around d_c, we employ SC approximation which is equivalent to ignoring the coupling between different configurations.[8] The use of this approach is really justified because the only $|\sigma_g^{\uparrow}\sigma_u^{\downarrow}\rangle - |\sigma_g^{\downarrow}\sigma_u^{\uparrow}\rangle$ configuration contributes to the ${}^1\Sigma_g^{(a)}$ state at the anticrossing point [Fig. 8(a)]. In the SC approximation, the two-particle states have simple analytical solutions,[8]

$$E({}^1\Sigma_g^{(a)}) = E_g + E_u + V_{gu} + K_{gu} \tag{5}$$

for the $|\sigma_g^{\uparrow}\sigma_u^{\downarrow}\rangle - |\sigma_g^{\downarrow}\sigma_u^{\uparrow}\rangle$ singlet state and

$$E({}^3\Sigma_u) = E_g + E_u + V_{gu} - K_{gu} \tag{6}$$

for ${}^3_+\Sigma_u$, ${}^3_-\Sigma_u$, and ${}^3_0\Sigma_u$ triplet states. Hence, the singlet-triplet splitting is given by

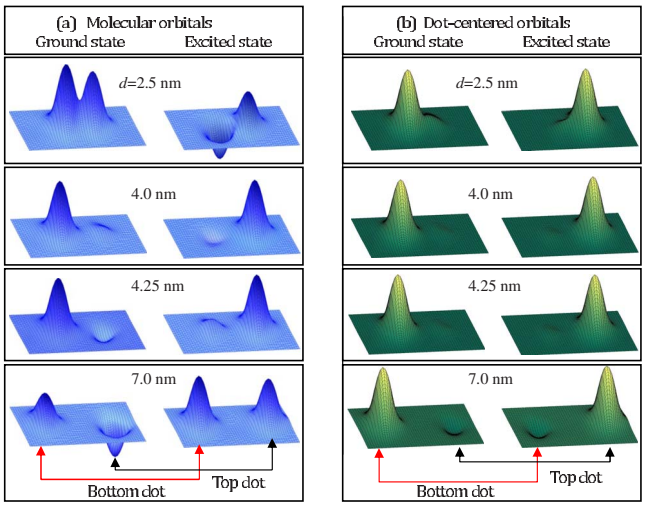

FIG. 10. (Color online) Spatial distributions of (a) single-particle molecular orbitals and (b) single-particle dot-centered hole wave functions in the (yz) plane. The z axis goes though the vertical symmetry axis of the pyramids. As a typical example of the hole states, we depict the $|\frac{3}{2},-\frac{3}{2}\rangle$ component for $l=15$ nm. The dot-centered orbitals are obtained from a unitary rotation of the molecular states [Eq. (8)]. Note the change in the ground-state symmetry of the molecular orbital between 4.0 and 4.25 nm and localization of the ground and excited states in opposite dots.

$$J_{ST} = E({}^1\Sigma_g^{(a)}) - E({}^3\Sigma_u) = 2K_{gu}. \tag{7}$$

As it follows from the antisymmetry of the total wave function for particle permutation, the energy gap between the $|\sigma_g^{\uparrow}\sigma_u^{\downarrow}\rangle - |\sigma_g^{\downarrow}\sigma_u^{\uparrow}\rangle$ singlet and the $|\sigma_g^{\uparrow}\sigma_u^{\downarrow}\rangle + |\sigma_g^{\downarrow}\sigma_u^{\uparrow}\rangle$ triplet is an exchange energy; hereby the result (7) gets a simple interpretation. At $d=d_c$, the exchange integral is equal to zero and $J_{ST}\to 0$.

It now remains to explain why the exchange energy K_{gu} vanishes and the configuration $|\sigma_g^{\uparrow}\sigma_u^{\downarrow}\rangle - |\sigma_g^{\downarrow}\sigma_u^{\uparrow}\rangle$ dominates at the crossing/anticrossing point. The main reason for the hole states to behave so differently than the electron states is traced in effect of strain on single-particle hole states, which is illustrated in Figs. 9–11. It is of importance that close to d_c the ground state (σ_g or σ_u depending on d) becomes progres-

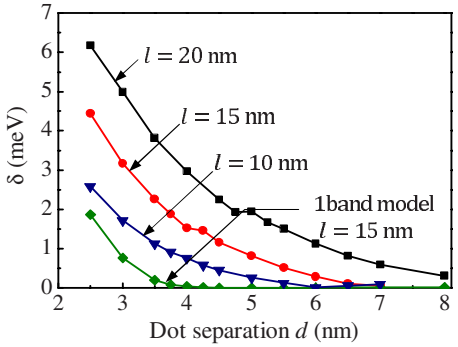

FIG. 11. (Color online) The splitting between the lowest single-particle energy levels on the bottom (e_B) and top (e_T) dots, $\delta=e_B-e_T$, obtained using a 6×6 $\mathbf{k}\cdot\mathbf{p}$ model ($l=10$, 15, and 20 nm) and a single-band approximation ($l=15$ nm) with Eq. (9).

sively localized in the bottom dot while the excited state tends to occupy the top dot (Fig. 9). Asymmetry of strain-field distribution exerted by the presence of the other dot, makes the geometrically identical QDs to be nonidentical.[7,21,33,37,44] The biaxial strain in the bottom Ge dot is larger than in the top dot (Fig. 3). Such strain asymmetry promotes stronger localization of the ground hole state in the bottom dot (Fig. 10) and leads to the energy difference between the dot-centered orbitals, $\delta = e_B - e_T$.

To estimate δ, we resort to a Wannier-type transformation of molecular orbitals to the dot-centered states.[7,8] The dot-centered basis ϕ_η can be obtained from a unitary rotation of molecular orbitals ψ_i, i.e.,

$$\phi_\eta = \sum_i U_{\eta i}\psi_i, \tag{8}$$

where $U_{\eta i}$ is a unitary matrix chosen to maximize the total self-Coulomb energy. The procedure of finding matrices $U_{\eta i}$ is described in detail in Ref. 8. Once we have U, we can define the effective single-particle energies of dot-centered states as

$$e_\eta = \sum_i U^*_{\eta i} U_{\eta i} E_i, \tag{9}$$

where E_i is the energy of the ith molecular orbital. Figure 11 shows the energy separation of the two lowest single-dot energies e_B and e_T obtained in the Wannier representation for QDs with different sizes. For comparison, we plot also the data obtained with one-band heavy-hole approximation. We see that δ rises quickly as the interdot distance is reduced and as the dot size is increased due to enhancement of strain asymmetry. Strain asymmetry has a weak effect on δ in one-band approximation and yields the large energy separation in a six-band model. A possible reason of a such difference is discussed in Appendix.

In a simplest scenario, for nonidentical QDs the states σ_g and σ_u split with an energy difference $|\sigma_{gu}| = \sqrt{\Delta_T^2 + \delta^2}$, where Δ_T is the quantum-mechanical coupling energy. Hole tunneling makes it advantageous to create the molecular states delocalized over two dots with the positive-energy splitting between σ_g and σ_u. The difference of the original energy levels of the two dots, however, tends to separate holes. Since the bonding and antibonding orbitals are formed by different combinations of HH, LH, and SO states,[21] they are shifted in a different way under the action of strain, i.e., the biaxial strain also tends to split the single-particle hole states. However, in this case, the splitting of σ_g and σ_u is negative as the strain affects stronger the position of σ_u state, shifting it closely to the conduction band as compared to σ_g. This follows from the fact that antibonding state has a suppressed amplitude in the barrier and hence contains larger contribution of the HH component and smaller contribution of LH and SO.[21,22] At small interdot distance, the quantum-mechanical coupling energy wins, and both bonding and antibonding orbitals are extended quasiequally in both dots. However, increasing dot separation tends to reduce Δ_T rapidly so at some point the factor of the long-range strain asymmetry wins and the hole states start to occupy different dots. In this weak-coupling region, strain-induced shifts of the hole subbands dominate over tunneling splitting. In Ge regions, biaxial strain is positive. Therefore, σ_u is more shifted toward the conduction band than the bonding state, eventually replacing σ_g and causing single-particle level crossing. Finally, at large d, both Δ_T and δ vanish and the asymmetry of single-particle molecular states diminishes (Fig. 10).

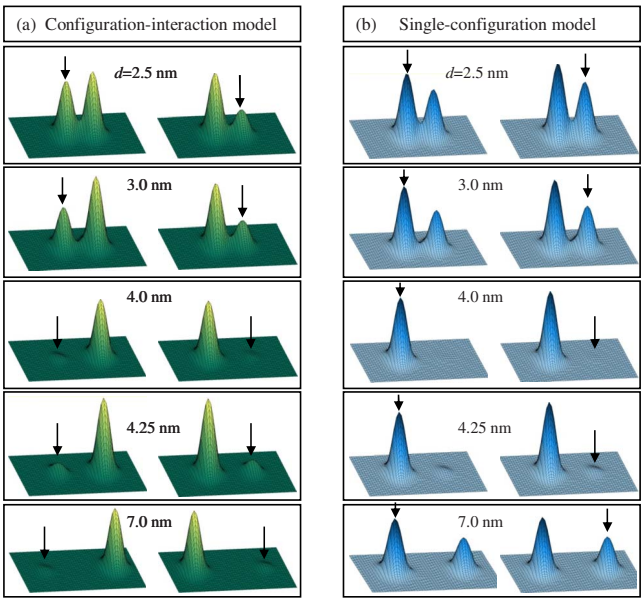

FIG. 12. (Color online) Comparison of pair-correlation functions calculated using (a) configuration-interaction method and (b) single-configuration approximation for the ground-state singlet ${}^1\Sigma_g^{(a)}$ at several selected d and $l=15$ nm. On the left-hand sides of panels (a) and (b), the first hole is fixed at the maximum of the charge density of the bottom dot while on the right-hand sides, the first hole is fixed at the maximum of the charge density of the top dot, as indicated by the arrows. At the SC level, the lowest singlet state corresponds to $|\sigma_g^\uparrow \sigma_g^\downarrow\rangle$ for $d < d_c$ and to $|\sigma_u^\uparrow \sigma_u^\downarrow\rangle$ for $d > d_c$.

The phenomenon of localization of single-particle orbitals on different dots plays an important role also in many-particle states. First, the energy cross integrals V_{gu} and K_{gu} drop near d_c because they correspond to σ_g and σ_u states confined in remote QDs. Opposite trends apply to V_{gg} and V_{uu}. The self-Coulomb energies V_{gg} and V_{uu} are mainly due to intradot interaction and therefore increase in this region (Fig. 8). Second, at the crossing point σ_g and σ_u states are degenerate. In this case, the many-particle wave function is constructed from the single-dot orbitals ϕ_η centered on different QDs to minimize Coulomb repulsion between two holes. For example, ${}^1\Sigma_g^{(a)} = |\phi_B^\uparrow \phi_T^\downarrow\rangle - |\phi_B^\downarrow \phi_T^\uparrow\rangle$. Since at $d \sim d_c$, the dot-centered basis coincides with the basis of molecular orbitals (Fig. 10), the ground-state singlet is nothing but the $|\sigma_g^\uparrow \sigma_u^\downarrow\rangle - |\sigma_g^\downarrow \sigma_u^\uparrow\rangle$ configuration.

To explore spatial symmetry of the many-particle states in more detail, we study the pair-correlation functions for the ground-state singlet ${}^1\Sigma_g^{(a)}$ obtained within the configuration-interaction and single-configuration approaches. Results are plotted in Fig. 12. As expected for the SC approximation, the many-particle state exhibits *no spatial correlations* among the two holes: the second hole tends to occupy the bottom

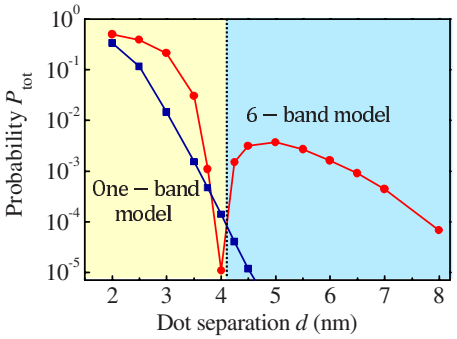

FIG. 13. (Color online) The probability of two holes occupying the same dot, P_{tot}, calculated from single-band and multiband models for the ground-state singlet ${}^1\Sigma_g^{(a)}$ ($l=15$ nm). Here $P_{tot}=P_{BB}+P_{TT}$, where P_{BB} (P_{TT}) is the probability of both holes being on the bottom (top) dot. The vertical dot line indicates the distance d_c at which the level crossing/anticrossing occurs.

dot irrespective of the position of the first one. Note that at the SC level, the lowest singlet state corresponds to $|\sigma_g^{\uparrow}\sigma_g^{\downarrow}\rangle$ configuration for $d<d_c$ and to $|\sigma_u^{\uparrow}\sigma_u^{\downarrow}\rangle$ for $d>d_c$. The obvious tendency for the two holes to reside in the bottom dot originates from the strain-induced asymmetry in their single-particle states [compare Figs. 10 and 12(b)]. In contrast, once the configuration interaction is introduced, the two holes are each localized on different dots above a certain interdot separation [Fig. 12(a)], showing spatial correlations.

To identify the contribution of strain-induced asymmetry of single-particle states to the asymmetry of many-particle wave functions, we analyze the dot double occupancy which is the probability of two holes occupying the dot $\eta=T$ or B at the same time. To obtain the bihole localization parameters, we solve the CI problem in the dot-centered Wannier basis ϕ_η and find the probability of two holes simultaneously occupying the top or bottom dots as the weight of the respective configuration in the many-particle wave function.[7] The possible spin configurations in Wannier basis are $|\phi_B^{\uparrow}\phi_T^{\uparrow}\rangle$, $|\phi_B^{\downarrow}\phi_T^{\downarrow}\rangle$, $|\phi_B^{\uparrow}\phi_T^{\downarrow}\rangle$, $|\phi_B^{\downarrow}\phi_T^{\uparrow}\rangle$, $|\phi_B^{\uparrow}\phi_B^{\downarrow}\rangle$, and $|\phi_T^{\uparrow}\phi_T^{\downarrow}\rangle$. Thus, the weight of the $|\phi_B^{\uparrow}\phi_B^{\downarrow}\rangle$ determinant gives the probability of both holes being on the bottom dot, P_{BB} while the weight of the $|\phi_T^{\uparrow}\phi_T^{\downarrow}\rangle$ configuration provides P_{TT}. Figure 13 shows the total double-occupancy probability $P_{tot}=P_{BB}+P_{TT}$ of the first singlet state obtained from single-band calculations (weak asymmetry of single-particle orbitals) and multiband model (strong asymmetry of single-particle states). At small d, the both approaches give $P_{tot}\approx 0.4-0.5$ as the two holes are delocalized into two dots. In the absence of asymmetry in σ_g and σ_u (or the asymmetry is rather weak), the coupling between $|\sigma_g^{\uparrow}\sigma_g^{\downarrow}\rangle$ and $|\sigma_u^{\uparrow}\sigma_u^{\downarrow}\rangle$ configurations yields the separation of holes at practically any d (except the shortest ones), thus exponentially decreasing the double hole occupation. In the six-band $\mathbf{k}\cdot\mathbf{p}$ model, the delocalized-to-localized transition occurs at larger dot separation due to admixture of the light and split-off states and thereby smaller effective mass. Therefore, P_{tot} calculated within the multiband approach is, in general, a weaker function of d. However, at $d\approx d_c$ the ground-state singlet consists of a single configuration $|\sigma_g^{\uparrow}\sigma_u^{\downarrow}\rangle-|\sigma_g^{\downarrow}\sigma_u^{\uparrow}\rangle$ with σ_g and σ_u orbitals being entirely localized on different dots. Evidently, for such a configuration both the correlation and strain asymmetry lead to a dramatic drop of the double hole occupation. The local minimum at $d\sim 4$ nm is a consequence of this effect.

IV. CONCLUSIONS

Hole states confined in two vertically coupled Ge/Si quantum dots are analyzed using a strain-dependent six-band $\mathbf{k}\cdot\mathbf{p}$ model combined with the configuration-interaction method. This approach permits an accurate treatment of the direct Coulomb and exchange interaction, as well as the correlation effects by allowing interconfiguration coupling. In the two-hole system, the ground state is a spin-singlet state followed by a threefold-degenerate triplet state, where the term "spin" is an index for two Kramers degenerate states. As the space between dots increases, the singlet-triplet splitting drops to zero and then restores again, implying level anticrossing with a zero anticrossing energy gap. We demonstrate that the many-particle level anticrossing occurs at the interdot distance at which the single-particle ground state changes its symmetry from bonding to antibonding. The results are interpreted in terms of asymmetry-induced localization of single-particle orbitals caused by the interplay of effects of strain and hole subband mixing. The symmetry breaking for many-particle states as a joint action of correlations and strain is observed with an increasing dot separation. We hope these results may inspire further investigation exploring the singlet-triplet entanglement in two-hole systems for possible device applications.

ACKNOWLEDGMENTS

The authors are much obliged to A. F. Zinovieva and A. V. Nenashev for very helpful discussions. This work was supported by RFBR (Grant No. 09-02-00050) and Integration Project No. 1.13.20. A.A.B. acknowledges financial support of the Dynasty Foundation.

APPENDIX

We now comment on a possible explanation of why the strain-induced asymmetry of single-hole states in multiband model is larger than in one-band approximation. For biaxial

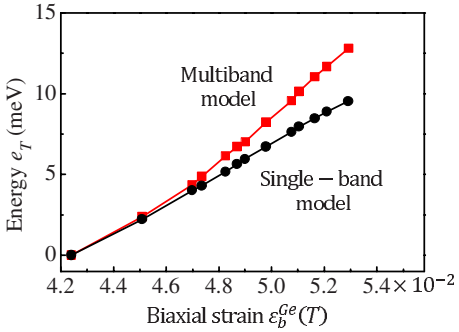

FIG. 14. (Color online) The strain-induced energy shift of single-particle orbital localized on the top dot for single-band and multiband calculations and $l=15$ nm. The energies are counted with respect to their values e_T at $d=2.5$ nm.

strain along [001] orientation, the model-solid theory[45] predicts the following strain-induced energy shifts with respect to the average valence-band energy:

$$\Delta E_{\mathrm{HH}} = |b|\varepsilon_b, \tag{A1}$$

$$\Delta E_{\mathrm{LH}} = -\Delta E_{\mathrm{HH}} - 0.5[(\Delta_0 - \Delta E_{\mathrm{HH}}) - \sqrt{(\Delta_0 - \Delta E_{\mathrm{HH}})^2 + 8(\Delta E_{\mathrm{HH}})^2}], \tag{A2}$$

$$\Delta E_{\mathrm{SO}} = -\Delta E_{\mathrm{HH}} - 0.5[(\Delta_0 - \Delta E_{\mathrm{HH}}) + \sqrt{(\Delta_0 - \Delta E_{\mathrm{HH}})^2 + 8(\Delta E_{\mathrm{HH}})^2}], \tag{A3}$$

where $|b|$ is the deformation potential, $\varepsilon_b = \varepsilon_{zz} - 0.5(\varepsilon_{xx} + \varepsilon_{yy})$ is the biaxial strain, and Δ_0 is the constant of spin-orbit splitting. When the hole state in a quantum dot is formed by the heavy-hole subband only, the position of hole energy level is simply a linear function of biaxial strain inside the dot [Eq. (A1)]. The behavior becomes more complicated when one takes into account the admixture of the light and split-off states. The biaxial strain in the Ge nanocluster leads to splitting between HH and LH (SO) states [see Eqs. (A1)–(A3)]. As a result, the contribution of HH subband to the hole state increases and the admixture of LH and SO states decreases as the strain is increased. This means that the energy of many-component hole states depends on strain stronger than a linear law. Therefore, the strain-asymmetry-induced energy difference between the dot-centered levels computed with a multiband approach is larger than that calculated with a one-band approximation. In Fig. 14, we plot the energy of single-particle orbital localized on the top dot (e_T) as a function of $\varepsilon_b^{\mathrm{Ge}}(T)$ for single-band and multiband calculations. Clearly, these two dependencies differ from one another in a predicted way, providing support for our explanation.

*yakimov@isp.nsc.ru

[1] D. Loss and D. P. DiVincenzo, Phys. Rev. A **57**, 120 (1998).
[2] G. Burkard, D. Loss, and D. P. DiVincenzo, Phys. Rev. B **59**, 2070 (1999).
[3] X. Hu and S. Das Sarma, Phys. Rev. A **61**, 062301 (2000).
[4] R. Hanson and G. Burkard, Phys. Rev. Lett. **98**, 050502 (2007).
[5] A. Barenco, C. H. Bennett, R. Cleve, D. P. DiVincenzo, N. Margolus, P. Shor, T. Sleator, J. A. Smolin, and H. Weinfurter, Phys. Rev. A **52**, 3457 (1995).
[6] M. Rontani, F. Troiani, U. Hohenester, and E. Molinari, Solid State Commun. **119**, 309 (2001).
[7] L. He, G. Bester, and A. Zunger, Phys. Rev. B **72**, 081311(R) (2005).
[8] L. He, G. Bester, and A. Zunger, Phys. Rev. B **72**, 195307 (2005).
[9] D. V. Melnikov and J.-P. Leburton, Phys. Rev. B **73**, 155301 (2006).
[10] D. V. Melnikov, J.-P. Leburton, A. Taha, and N. Sobh, Phys. Rev. B **74**, 041309(R) (2006).
[11] J. Z. García, P. Pietiläinen, H.-Yi Chen, and T. Chakraborty, Physica E **40**, 2839 (2008).
[12] A. V. Khaetskii and Y. V. Nazarov, Phys. Rev. B **61**, 12639 (2000).
[13] L. M. Woods, T. L. Reinecke, and Y. Lyanda-Geller, Phys. Rev. B **66**, 161318(R) (2002).
[14] J. L. Cheng, M. W. Wu, and C. Lü, Phys. Rev. B **69**, 115318 (2004).
[15] A. M. Alcalde, Q. Fanyao, and G. E. Margues, Physica E **20**, 228 (2004).
[16] D. Klauser, W. A. Coish, and D. Loss, Phys. Rev. B **73**, 205302 (2006).
[17] D. Heiss, S. Schaeck, H. Huebl, M. Bichler, G. Abstreiter, J. J. Finley, D. V. Bulaev, and D. Loss, Phys. Rev. B **76**, 241306(R) (2007).
[18] C. Lü, J. L. Cheng, and M. W. Wu, Phys. Rev. B **71**, 075308 (2005).
[19] D. V. Bulaev and D. Loss, Phys. Rev. Lett. **98**, 097202 (2007).
[20] A. V. Nenashev, A. V. Dvurechenskii, and A. F. Zinovieva, Phys. Rev. B **67**, 205301 (2003).
[21] A. I. Yakimov, A. A. Bloshkin, and A. V. Dvurechenskii, Phys. Rev. B **78**, 165310 (2008).
[22] A. I. Yakimov, A. A. Bloshkin, and A. V. Dvurechenskii, Semicond. Sci. Technol. **24**, 095002 (2009).
[23] J. I. Climente, M. Korkusinski, G. Goldoni, and P. Hawrylak, Phys. Rev. B **78**, 115323 (2008).
[24] M. F. Doty, J. I. Climente, M. Korkusinski, M. Scheibner, A. S. Bracker, P. Hawrylak, and D. Gammon, Phys. Rev. Lett. **102**, 047401 (2009).
[25] C.-Y. Hsieh, R. Cheriton, M. Korkusinski, and P. Hawrylak, Phys. Rev. B **80**, 235320 (2009).
[26] H. W. van Kesteren, E. C. Cosman, W. A. J. A. van der Poel, and C. T. Foxon, Phys. Rev. B **41**, 5283 (1990).
[27] X. Marie, T. Amand, P. Le Jeune, M. Paillard, P. Renucci, L. E. Golub, V. D. Dymnikov, and E. L. Ivchenko, Phys. Rev. B **60**, 5811 (1999).
[28] A. F. Zinovieva, A. V. Nenashev, and A. V. Dvurechenskii, Phys. Rev. B **71**, 033310 (2005).
[29] K. V. Kavokin, Phys. Rev. B **69**, 075302 (2004).
[30] A. I. Yakimov, A. I. Nikiforov, A. V. Dvurechenskii, V. V. Ulyanov, V. A. Volodin, and R. Groetzschel, Nanotechnology **17**, 4743 (2006); A. I. Yakimov, G. Yu. Mikhalyov, A. V. Dvurechenskii, and A. I. Nikiforov, J. Appl. Phys. **102**, 093714 (2007).
[31] A. I. Yakimov, A. V. Dvurechenskii, and A. I. Nikiforov, J. Nanoelectron. Optoelectron. **1**, 119 (2006).
[32] S. Christiansen, M. Albrecht, and H. P. Strunk, Appl. Phys. Lett. **64**, 3617 (1994).
[33] A. I. Yakimov, G. Yu. Mikhalyov, and A. V. Dvurechenskii, Nanotechnology **19**, 055202 (2008).
[34] G. L. Bir and G. E. Pikus, *Symmetry and Strain-Induced Effects in Semiconductors* (Wiley, New York, 1974).
[35] L. G. C. Rego, P. Hawrylak, J. A. Brum, and A. Wojs, Phys. Rev. B **55**, 15694 (1997).
[36] G. Bester, A. Zunger, and J. Shumway, Phys. Rev. B **71**, 075325 (2005).
[37] W. Jaskólski, M. Zieliński, G. W. Bryant, and J. Aizpurua, Phys. Rev. B **74**, 195339 (2006).

[38] M. F. Doty, M. Scheibner, A. S. Bracker, I. V. Ponomarev, T. L. Reinecke, and D. Gammon, Phys. Rev. B **78**, 115316 (2008).
[39] C. Yannouleas and U. Landman, Phys. Rev. Lett. **82**, 5325 (1999).
[40] R. M. Abolfath and P. Hawrylak, Phys. Rev. Lett. **97**, 186802 (2006).
[41] B. Partoens and F. M. Peeters, Phys. Rev. Lett. **84**, 4433 (2000).
[42] D. V. Melnikov and J. P. Leburton, Phys. Rev. B **73**, 085320 (2006).
[43] At $d \approx d_c$, the ${}^1\Sigma_g^{(a)}$ and ${}^3\Sigma_u$ states are degenerate.
[44] W. Sheng and J.-P. Leburton, Phys. Rev. Lett. **88**, 167401 (2002).
[45] F. H. Pollak and M. Cardona, Phys. Rev. **172**, 816 (1968).